Somite deformations buffer imprecise segment lengths to ensure left-right symmetry

Sundar R. Naganathan,[1*] Marko Popović,[2] Andrew C. Oates [1*]

[1]Institute of Bioengineering, École Polytechnique Fédérale de Lausanne, CH 1015, Switzerland
[2]Institute of Physics, École Polytechnique Fédérale de Lausanne, CH 1015, Switzerland

[*]To whom correspondence should be addressed
E-mail: sundar.naganathan@epfl.ch, andrew.oates@epfl.ch

The body axis of vertebrate embryos is periodically segmented into bilaterally symmetric pairs of somites. The anteroposterior length and boundary position of somites are thought to be molecularly determined prior to somite morphogenesis. We show that in zebrafish embryos, initial somite lengths and positions are imprecise and many somites form left-right asymmetrically. Yet, within an hour, lengths are adjusted, becoming more symmetric, through somite deformations occurring independently on the left and right sides of the embryo. This adjustment is directed by a combination of somite surface tension, external stresses from neighbouring tissues and convergence-extension flows within somites. The ensuing left-right symmetry in somite boundary positions follows as a straightforward consequence of the length adjustments. Thus, the precision and symmetry of a fundamental embryonic morphological pattern is ensured by tissue mechanics.

Vertebrates are characterized by a left-right symmetric musculoskeletal system that emerges

from bilateral somites during embryonic development. Somites are 3D multicellular units, typically with an outer epithelial layer surrounded by a fibronectin-rich extracellular matrix, that form by segmentation of the presomitic mesoderm (PSM) (*1, 2*). Errors in setting their anteroposterior (AP) lengths affect downstream musculoskeletal morphogenesis (*3–5*) and left-right (LR) asymmetries of the musculoskeletal system have often been observed in scoliosis patients (*6, 7*). The AP length of somites and their LR symmetry is generally thought to be determined in the unsegmented PSM by genetic oscillations of a segmentation clock and downstream molecular prepatterns (*1, 2, 8–12*). While mechanical processes have also been associated with somite morphogenesis (*13–17*), their role in determining AP length and LR symmetry, if any, is not understood. In general, a quantitative study of bilateral symmetry in somites is lacking owing to the technical difficulty in following 3D somite morphogenesis simultaneously on the left and right sides of embryos.

To study LR somite morphogenesis in real time, we performed multiview light-sheet microscopy of zebrafish embryos (Fig. S1, S2, Movie S1, S2) and first quantified the AP length, L_{AP} (Fig. 1A, Fig. S3), of somites one to eight. We observed that the initial L_{AP}, immediately after somite formation, was variable (Fig. 1B, Fig. S4A; Coefficient of Variation, CV, 0.12; 95% CI [0.11,0.14]). To check whether the molecular prepatterns that are thought to set L_{AP} can explain this variability, we measured interstripe distance in *mespb* gene expression stripes, which represent the first molecular indication of segment length in the anterior PSM (*18*). We observed the variability in L_{AP} to be similar in magnitude to that of *mespb* segmental lengths (Fig. 1, D and E), suggesting that imprecision in L_{AP} could be the consequence of a variable prepattern. Strikingly, within an hour after somite formation, L_{AP} adjusted and the variability decreased (Fig. 1B; CV, 0.08 [0.07,0.09]; Fig. S4). By comparing the initial and one-hr lengths, we identified $L^0_{AP} = 53\ \mu m$ (Fig. 1C), which we defined as the target AP length, towards which

somites tended to adjust. In other words, somites with $L_{AP} > L^0_{AP}$ tended to become smaller and vice versa.

To investigate the mechanism of L_{AP} adjustment, we first asked whether L_{AP} on one side is influenced by lengths on the contralateral side. Comparing temporal changes in length between corresponding LR somites, we observed that only somites with an initial length away from L^0_{AP} adjusted their lengths (Fig.1, F and G). In contrast, somites that formed with initial L_{AP} close to L^0_{AP} changed negligibly. Importantly, length changes occurred on the two sides only when initial L_{AP} on both sides were away from L^0_{AP} (Fig. 1, H and I). Combined, these results suggest that L_{AP} changes are not driven by comparisons to the contralateral side, but rather are independently determined by whether or not a particular somite has an initial length close to the target length.

To check whether the presence of correctly formed somites on the contralateral side is required, we injected dominant negative (DN) *fibronectin 1a* mRNA together with DN *fibronectin 1b* in one of the cells at the 2-cell stage (Fig. 1J), which has been previously shown to perturb somite formation on one side (*19*). Injections resulted in 10% of the embryos bearing strongly disrupted somites on one side (Fig. 1J). When L_{AP} of somites three to six was analyzed in the somite-forming side, we observed that lengths adjusted towards the same L^0_{AP} similar to uninjected embryos, despite the absence of somites on the contralateral side (Fig. 1K). While a possible cross talk mediated by fibronectin between the LR sides has been suggested (*20*), our results indicate that L_{AP} adjustment on one side does not require somite morphogenesis in the contralateral side.

We next asked whether L_{AP} adjustment is accompanied by a change in cell number or

somite volume. Even though cell numbers increased in all somites in the one-hour analysis period (Fig. S5B), we observed no significant correlation (r, -0.18 [-0.47,0.1]) between change in cell number and change in L_{AP} (Fig. 2A). Moreover, somites exhibited a negligible change in volume (Fig. 2, B and C). This suggests that L_{AP} adjustment must be reflected in corresponding changes in the other two dimensions of the somite. We therefore quantified 3D shape changes (Supplementary Materials) and observed that mediolateral (ML) somite lengths decreased over time, while dorsoventral (DV) lengths increased, reflecting convergence-extension (CE) in somites (Fig. 2, D-F, Fig. S5). The initial L_{AP} was positively correlated (r, 0.51 [0.27,0.68]) with relative changes in ML length (Fig. 2G). Thus, somites with a smaller L_{AP} tended to have an increased reduction of ML length and vice versa. In contrast, initial L_{AP} was not correlated (r, 0.02 [-0.25,0.3]) with relative changes in DV length (Fig. 2H). These results suggest that DV length dynamics do not contribute to L_{AP} adjustment. Consequently, given the conservation of volume, adjustments in L_{AP} are buffered by ML shape changes. These observations suggest that AP length robustness is associated with mechanical forces that drive somite shape changes.

To understand if mechanical forces are sufficient for L_{AP} adjustment, we next sought to develop a coarse-grained mechanical model of a newly formed somite, which we represent as a cuboid of constant volume (Fig. 3D(a)). Mechanical stresses acting on the somite consist of somite surface tension stemming from both extracellular matrix and somite epithelial cells, contact stresses with surrounding tissues and internal active stresses driving CE flows. How these stresses lead to somite shape changes is determined by the somite material properties, which we investigated by culturing a single somite isolated from the embryo (Fig. 3A). Interestingly, all explanted somites (N = 5) became spherical over time (Fig. 3B, Fig. S6, Movie S3) in the absence of neighbouring tissues. While the anterior PSM at later stages has been reported to

behave as a yield stress material (*21*), our results suggest that the explanted somite behaves as a viscous fluid with surface tension Γ (Fig. 3D(b)). Furthermore, the final spherical shape of explants suggests that organisation of internal active stresses in a somite is lost when explanted.

To investigate contact stresses in the AP dimension, we performed laser ablation of the PSM posterior to the most recently formed somite boundary. We observed that over time a bulge of the somite boundary next to the ablated site appeared, indicating that a compressive normal stress exists between the PSM and the somite (N = 6, Fig. 3C, Fig. S7). This is consistent with previous experiments in chick (*13*) and later stage zebrafish embryos (*22*). We include this stress in the model as normal stress $\sigma_a(t)$ acting on both the anterior and posterior surfaces of the somite (Fig. 3D(c)). Along DV dimension, somites are sandwiched between neural plate and yolk at early stages, imposing a constraint $l(t)$ on the DV extension of the somite (Fig. 3D(d)). Finally, we account for CE flows in the model through an internal active shear stress (*23, 24*). For simplicity, we do not specifically account for contact stresses along ML dimension (Supplementary Text) and we neglect frictional forces between somites and surrounding tissues.

Combining all these ingredients allows us to consider how a variation of AP length from the constant target value $\delta L_{AP} \equiv L_{AP} - L^0_{AP}$ evolves in time (Supplementary Text). We find,

$$\partial_t \delta L_{AP} \approx -\frac{2.1\Gamma}{L^0_{AP}\eta}\delta L_{AP} \quad , \tag{1}$$

where η is the somite viscosity and L^0_{AP} is determined by $\sigma_a(t)$, $l(t)$, internal active stresses and Γ. Therefore, variations of L_{AP} are reduced in time over the time-scale $\tau \approx \eta L^0_{AP}/(2.1\Gamma)$. Consistent with Eq. 1, we find that changes in L_{AP} *in vivo* are proportional to their initial values (Fig. 3E). A linear fit to the data yields the relaxation time-scale $\tau = 1.6 \pm 0.1$ hr. We then quantified the relaxation of explanted somites towards a spherical shape (Fig. 3F, Fig. S6) and

found τ_e to be 1.1 ± 0.4 hr, which is comparable to the L_{AP} relaxation time-scale τ (Supplementary Text). We conclude that even though L^0_{AP} is determined by a combination of surface tension, external stresses and CE flows, for a given L^0_{AP}, stresses generated by surface tension can account for a major part of the observed adjustment. Thus, imprecise somite lengths are tuned by tissue mechanics to ensure increased precision.

What is the consequence of these length adjustments for the bilateral symmetry of somites? We reasoned that if both the posterior boundary of the head mesoderm (*25*) and cell flow into the PSM are LR symmetric (*26*), length adjustments would simultaneously ensure LR symmetrical somite lengths and segment boundary positions along the body axis. We tested this expectation by first computing the AP length difference in left-right somite pairs. Initial length differences were variable without a bias in asymmetry between the two sides (CV, 0.1 [0.09,0.12]; Fig. 4, A and B), suggesting that many bilateral pairs form asymmetrically. The length difference decreased over time (CV, 0.07 [0.05,0.08]) and the initial variability in boundary position difference (CV, 0.12 [0.1,0.14]) also decreased (CV, 0.09 [0.07,0.1]; Fig. 4C). The initial length difference was positively correlated with posterior boundary position difference (r, 0.67 [0.51,0.8]) (Fig. 4E), but only weakly correlated with anterior boundary position difference (r, -0.24 [-0.45,-0.03]) (Fig. S9B). This indicates that as new somite pairs form, their anterior boundaries are symmetric, either because they were initially symmetric or because they had already adjusted, and any asymmetries in length are predominantly a result of asymmetric positioning of the most recently formed boundary. A change in position of the posterior boundary ensues, thus simultaneously leading to increased LR symmetry in both AP lengths and boundary positions (Fig. 4, D and F).

The AP length of somites has been understood from the perspective of the segmentation

clock and downstream molecular processes in the PSM, and bilateral somite formation has largely been considered to be symmetric (*27*). Asymmetry was thought to arise only when retinoic acid signalling was lost, exposing molecular prepatterns in the PSM to a gene expression program that determines left-sided organ positioning (*10–12, 28*). However, our findings that initial lengths are imprecise, but are adjusted by 3D somite deformations, show that this perspective is insufficient to describe the length and symmetry of somites. In addition to the prepattern, we argue that somite surface tension, external stresses from neighboring tissues and CE flows within somites must also be included. Similar to the hypothesis proposed in (*29*), our results suggest that the role of the prepattern is to provide a coarse allocation of material for each somite, which is then fine-tuned by tissue mechanics. The LR differences in somite formation observed here, in otherwise normally-developing wild type genetic backgrounds and in constant environmental conditions, reawakens the idea that links subtle developmental failures in left-right symmetry to idiopathic scoliosis in humans (*30*). Our work on 3D morphogenesis in vertebrate mesoderm joins recent studies of mechanical processes reported to buffer heterogeneous cell growth in sepals in plants (*31*) and to enable straight cephalic furrow formation in *Drosophila* embryonic epithelia (*32*), revealing mechanics as a general principle in ensuring developmental precision.

References

1. A. C. Oates, L. G. Morelli, S. Ares, *Development* **139**, 625 (2012).

2. S. R. Naganathan, A. C. Oates, *Seminars in Cell & Developmental Biology* (2020).

3. C. A. Henry, I. M. McNulty, W. A. Durst, S. E. Munchel, S. L. Amacher, *Developmental Biology* **287**, 346 (2005).

4. C. Schröter, A. C. Oates, *Current Biology* **20**, 1254 (2010).

5. Y. Harima, Y. Takashima, Y. Ueda, T. Ohtsuka, R. Kageyama, *Cell Reports* **3**, 1 (2013).

6. W. J. Wang, *et al.*, *Journal of Pediatric Orthopaedics* **31**, S14 (2011).

7. K. Kusumi, S. L. Dunwoodie, *The Genetics and Development of Scoliosis* (Springer Science+Business Media, New York, NY, 2018).

8. J. Cooke, E. C. Zeeman, *Journal of theoretical biology* **58**, 455 (1976).

9. I. Palmeirim, D. Henrique, D. Ish-Horowicz, O. Pourquié, *Cell* **91**, 639 (1997).

10. J. Vermot, *et al.*, *Science* **308**, 563 (2005).

11. J. Vermot, O. Pourquié, *Nature* **435**, 215 (2005).

12. Y. Kawakami, Á. Raya, R. M. Raya, C. Rodríguez-Esteban, J. C. I. Belmonte, *Nature* **435**, 165 (2005).

13. D. S. Packard, A. G. Jacobson, *Journal of Experimental Zoology* **207**, 81 (1979).

14. A. A. Dias, I. de Almeida, J. M. Belmonte, J. A. Glazier, C. D. Stern, *Science* **343**, 791 (2014).

15. J. B. L. Bard, *Roux's Archives of Developmental Biology* **197**, 513 (1988).

16. B. K. Nelemans, M. Schmitz, H. Tahir, R. M. Merks, T. H. Smit, *iScience* **23**, 100976 (2020).

17. R. Grima, S. Schnell, *Developmental Biology* **307**, 248 (2007).

18. T. Yabe, K. Hoshijima, T. Yamamoto, S. Takada, *Development* **143**, 2842 (2016).

19. J. Compagnon, *et al.*, *Developmental Cell* **31**, 774 (2014).

20. E. Guillon, *et al.*, *eLife* **9** (2020).

21. A. Mongera, *et al.*, *Nature* **561**, 401 (2018).

22. S. Tlili, *et al.*, *Proceedings of the National Academy of Sciences* **116**, 25430 (2019).

23. R. Etournay, *et al.*, *Elife* **4**, e07090 (2015).

24. M. Popović, *et al.*, *New Journal of Physics* **19**, 033006 (2017).

25. H. Wang, P. W. H. Holland, T. Takahashi, *EvoDevo* **10** (2019).

26. D. Das, V. Chatti, T. Emonet, S. A. Holley, *Developmental Cell* **42**, 170 (2017).

27. T. Brend, S. A. Holley, *Seminars in Cell & Developmental Biology* **20**, 472 (2009).

28. D. T. Grimes, *Development* **146** (2019).

29. C. D. Stern, R. Bellairs, *Journal of embryology and experimental morphology* **81**, 75 (1984).

30. C. J. Goldberg, E. E. Fogarty, D. P. Moore, F. E. Dowling, *Spine* **22**, 2228 (1997).

31. N. Hervieux, *et al.*, *Current Biology* **27**, 3468 (2017).

32. A. S. Eritano, *et al.*, *Developmental Cell* **53**, 212 (2020).

33. M. Weber, M. Mickoleit, J. Huisken, *Journal of Visualized Experiments* (2014).

34. J. Schindelin, *Nat. Methods* **9**, 676 (2012).

35. S. Preibisch, S. Saalfeld, J. Schindelin, P. Tomancak, *Nature Methods* **7**, 417 (2010).

36. A. F. Frangi, W. J. Niessen, K. L. Vincken, M. A. Viergever, *Medical Image Computing and Computer-Assisted Intervention — MICCAI'98*, W. M. Wells, A. Colchester, S. Delp, eds. (Springer Berlin Heidelberg, Berlin, Heidelberg, 1998), vol. 1496, pp. 130–137.

37. T. Pietzsch, S. Saalfeld, S. Preibisch, P. Tomancak, *Nature Methods* **12**, 481 (2015).

38. A. Sawada, *et al.*, *Development* **127**, 1691 (2000).

39. R. Narayanan, A. C. Oates, *Bio-protocol* **9** (2019).

40. A. Luciani, M. F. Champagne, L. A. Utracki, *Journal of Polymer Science Part B: Polymer Physics* **35**, 1393 (1997).

Acknowledgments

We thank members of the Oates lab, M. Gonzales-Gaitan, M. Labouesse, P. Tomancak, G. Salbreux, J. Bois, K. Uriu, V. Krishnamurthy, P. Gross and P. Chugh for comments on the manuscript; fish and bioimaging and optics core facility of École Polytechnique Fédérale de Lausanne. We acknowledge the vital early input of Chen Qian in the project. This work was supported by EPFL, Wellcome (WT098025MA); the Francis Crick Institute, receiving its core funding from Cancer Research UK, the Medical Research Council, and Wellcome; S.R.N. by a Long-Term Human Frontier Science Program postdoctoral fellowship (LT000078/2016); M.P. by the Swiss National Science Foundation Grant No. 200021-165509 and the Simons Foundation Grant No. 454953. S.R.N., M.P., and A.C.O. designed experiments, analyzed data and wrote the paper; S.R.N. performed experiments; M.P. developed theoretical model. The authors declare no competing interests. All data is available in the manuscript or the supplementary materials.

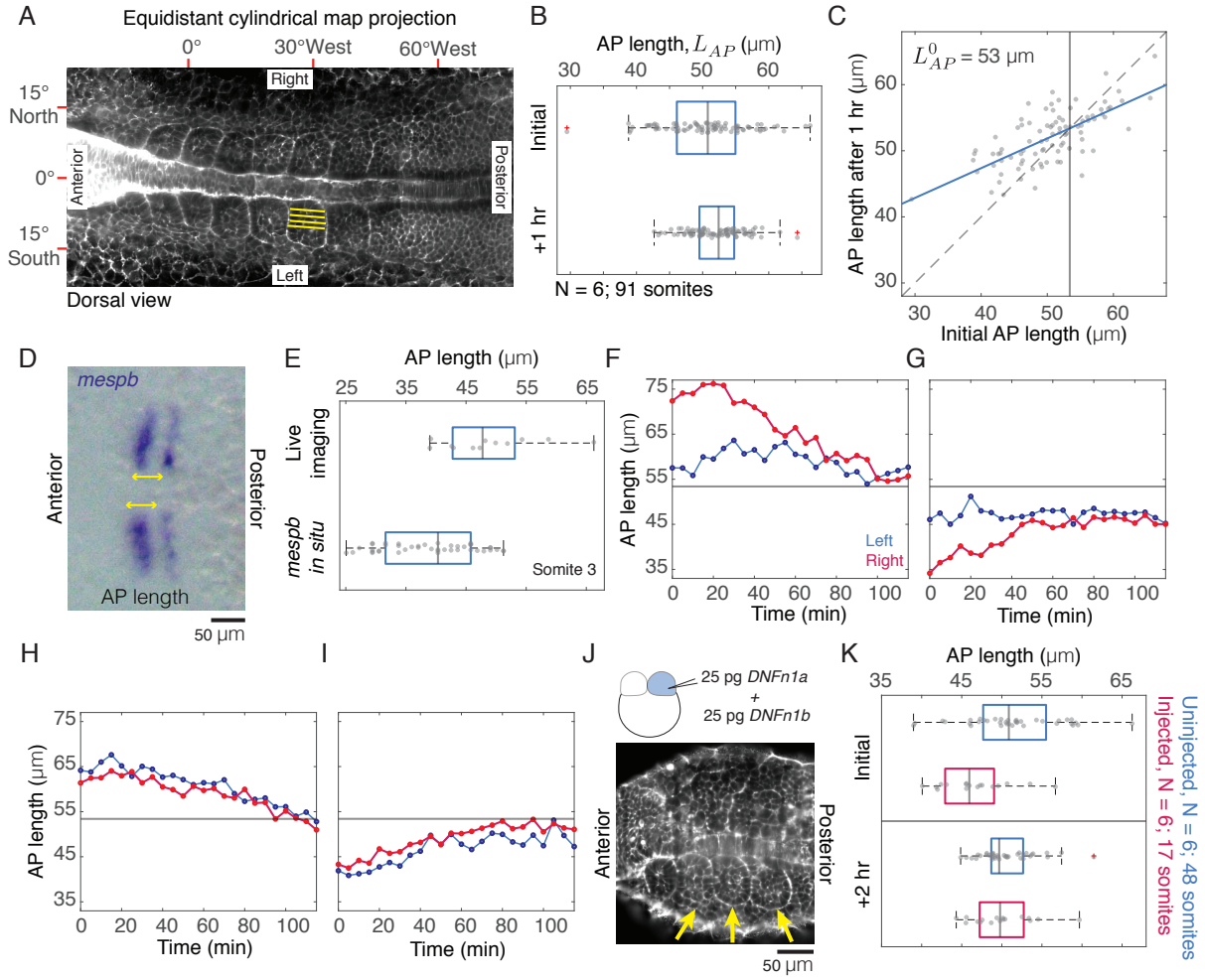

Figure 1: **Initial somite lengths are variable and get adjusted independently on the left-right sides** (A) Map projected image of a 6-somite stage zebrafish embryo. Yellow lines, AP length (L_{AP}) (B) Variability of L_{AP} of first eight somites decreases over time. (C) Comparison of initial and one-hour L_{AP}. Blue, linear regression; dashed line, slope=1; black line, target AP length, L^0_{AP} (D) Dorsal view of a flat-mounted embryo stained for *mespb* (blue). (E) Comparison of third somite L_{AP} measured from live imaging and *mespb in situ* (arrows in (D)). (F-I) Representative plots of LR somite pairs, where only somites with initial L_{AP} away from L^0_{AP} (black line) adjust their lengths. (J) Schematic, DN fibronectin injection at 2-cell stage. Representative embryo with somite formation on one side (arrows) and no visible somites on the contralateral side. (K) Comparison of L_{AP} of somites three-six in the somite-forming side of DN fibronectin injected embryos (red) and uninjected embryos (blue).

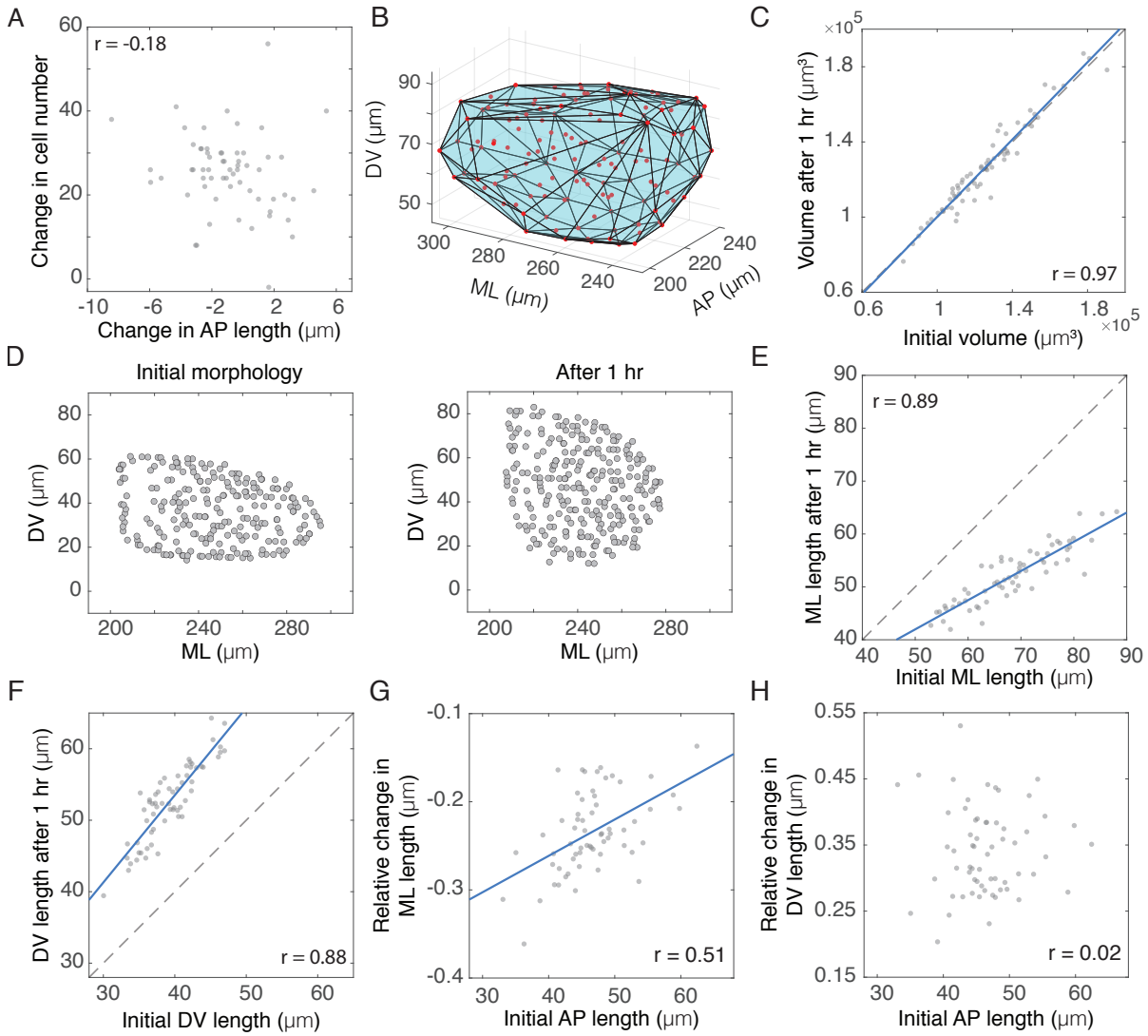

Figure 2: **AP length adjustment results from somite shape deformations** (A) Comparison of change in AP length and change in cell number. (B) Convex hull of segmented nuclei (red) from a single somite. (C) Comparison of initial and one-hour somite volumes (r, 0.97 [0.95,0.98]). Blue, linear regression in (C, E-G) and dashed line, slope=1 in (C, E, F). (D) Nuclei (circles) distribution of a somite undergoing convergence-extension. (E-F) Comparison of initial and one-hour ML and DV lengths indicate decrease (r, 0.89 [0.82,0.94) and increase (r, 0.88 [0.82,0.93]) in lengths respectively. (G-H) Initial AP lengths are positively correlated with relative changes in ML length $(L_{ML}(1hr) - L_{ML}(0hr))/L_{ML}(0hr)$ (G), and not correlated with relative changes in DV length $(L_{DV}(1hr) - L_{DV}(0hr))/L_{DV}(0hr)$ (H).

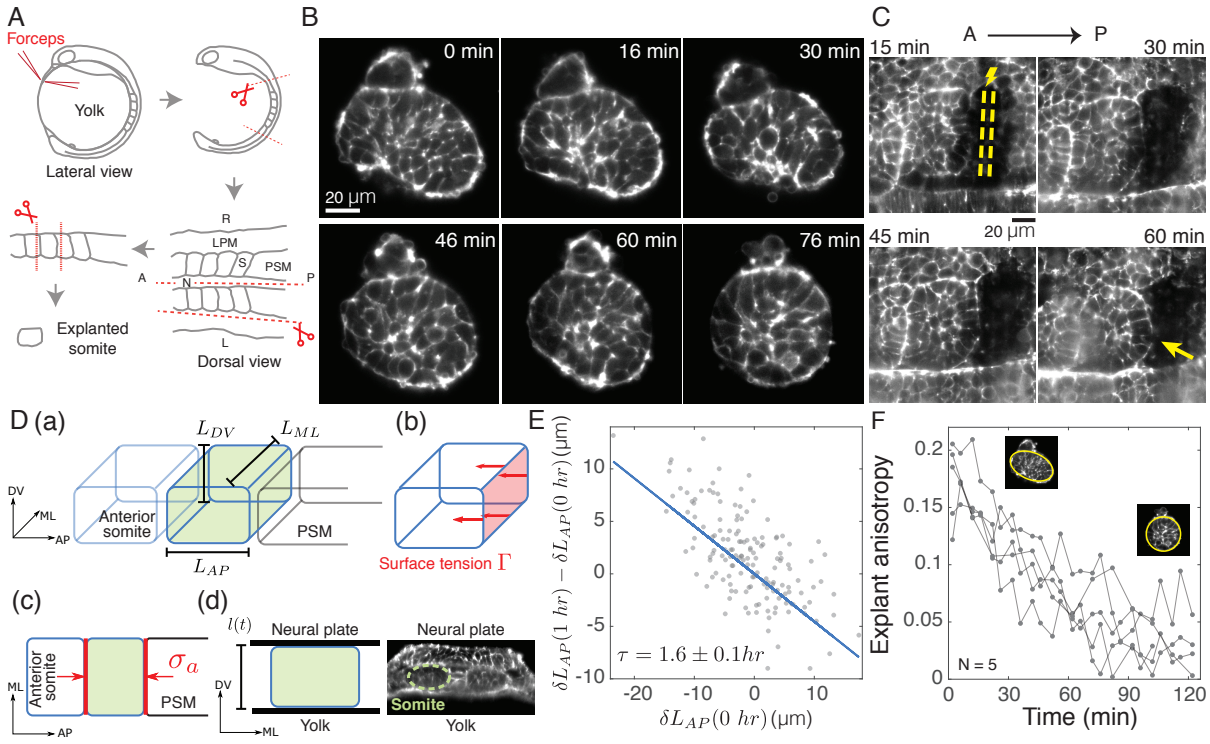

Figure 3: **Mechanics of somite shape changes**. (A) Schematic of somite explant preparation. A, anterior; P, posterior; L, left; R, right; PSM, presomitic mesoderm; LPM, lateral plate mesoderm; S, somite; N, notochord. (B) Explanted somite rounds up over time. (C) Ablation (yellow) of PSM adjacent to recently formed somite boundary. Yellow arrow, bulging of boundary. (D) (a) Schematic of somite dimensions. (b) Normal stress on somite surface due to surface tension. (c) Contacts (red) with PSM and anterior somite result in normal stress σ_a. (d) Left, constraint $l(t)$ imposed on L_{DV} by neural plate and yolk. Right, snapshot of somite 3 from a 3-somite stage embryo. (E) AP length adjustment during the first hour is proportional to the negative of its initial variation from L^0_{AP}, consistent with Eq. 1. Linear fit (blue) of the data yields the relaxation time-scale τ. (F) Shape anisotropy of explanted somites over time. Insets, representative initial and final shape.

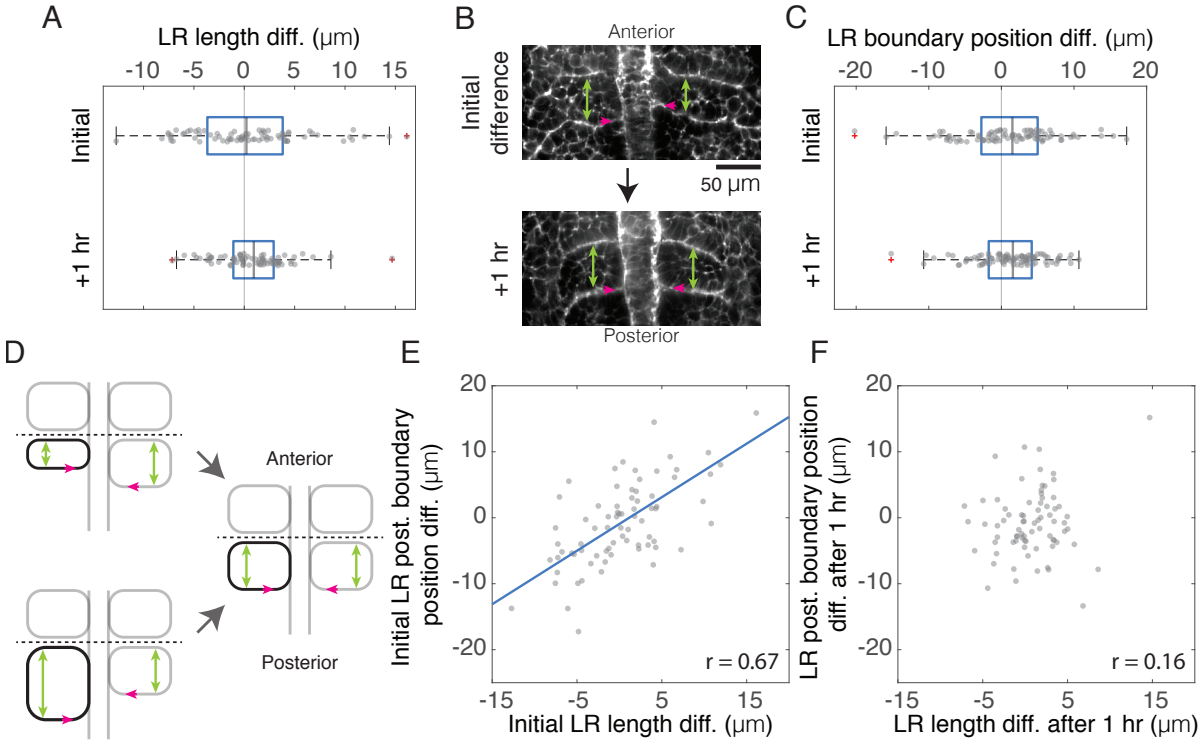

Figure 4: **Somite lengths and boundary positions increase symmetry over time**. (A) Variability in AP length difference between left-right somite pairs decreases over time. (B) Representative images of left-right somite pairs with asymmetric initial lengths (green) and somite boundary positions (pink) that adjust over time. (C) Variability in left-right boundary position difference decreases over time. (D) Schematic of initial asymmetries in somite length (green) and position (pink) adjusting concurrently. Dashed line represents aligned anterior boundaries. (E-F) AP length difference between left-right somite pairs is positively correlated initially with posterior boundary position difference (E), while no significant correlation is observed (r, 0.16 [-0.19,0.48]) after 1 hour (F). Blue, linear regression.